Stabilization of Thermosolutal Convective Instabilities in Ni-Based Single-Crystal Superalloys: Carbon Additions and Freckle Formation

S. TIN, T.M. POLLOCK, and W. MURPHY

The effect of carbon additions on the solidification characteristics of single-crystal Ni-based superalloys has been studied over a range of composition with large variations in Re, W, and Ta. Under constant processing conditions, nominally similar experimental alloys containing additions of 0.1 wt pct C exhibited a decreased tendency to develop grain defects, such as freckle chains. The carbon additions resulted in the formation of Ta-rich MC carbides with three distinct morphologies: blocky, nodular, and script. These carbides all precipitate near the liquidus temperature of the alloy. Intentional carbon additions also affected the segregation behavior of the constituent elements. Comparison of experimentally measured distribution coefficients assessed *via* application of a Scheil-type analysis revealed reduced segregation of Re, W, and Ta in experimental single-crystal alloys containing carbon. The mechanisms by which carbon additions influence freckle formation are considered.

I. INTRODUCTION

NICKEL-BASED single crystals are critical to the continued development of high-performance turbine engines, including aircraft engines and power-generation turbines. As the levels of refractory alloying additions to these materials have increased to improve high-temperature mechanical properties, grain-defect formation during directional solidification has become an increasingly important problem. Typically, grain defects, such as freckles and misoriented grains, are caused by the onset of thermosolutal convective instabilities due to dendritic segregation in these multicomponent alloys.[1–8] Preventing these defects is a major challenge, particularly when solidifying physically large, high-refractory-content crystals under inherently low thermal-gradient conditions.

Freckle formation has been a persistent problem in the solidification of single-crystal Ni-based superalloys since VerSnyder[9] pioneered the process in the 1960s. The presence of these undesirable grain defects, which lower the creep and fatigue properties, could potentially result in the premature failure of critical components. Early efforts taken to prevent these grain defects included the modification of gating designs and the application of high thermal gradients at the solidifying interface.[10] The onset of thermosolutal convection occurs when the buoyancy forces of the segregated solute in the interdendritic region exceed those of the surrounding viscous forces. Hence, by limiting the size of the channels in which solute can be accumulated through the adjustment of solidification parameters (the applied thermal gradient (G) and withdrawal rate (R)), the initiation of convective instabilities can be minimized.[1,3,11–15] Criteria for the development of convective instabilities have often been expressed in terms of dimensionless thermal and solutal Rayleigh numbers.[7,15] Making assumptions for the shape of the dendrite tip and accounting for primary dendrite arm spacing (PDAS) measurements in terms of G and R, the solutal Rayleigh number can be written as[3]

$$R_s = \frac{g\beta\phi}{9r^2 2\eta m_L D}\left(\frac{K}{GR}\right) \qquad [1]$$

where β is the solute volume-expansion coefficient, ϕ is the set of material parameters that relate to the PDAS selection, K is the permeability in a unidirectional temperature gradient, r is the dendrite tip radius, η is the viscosity, and D is the diffusivity. This expression suggests that the tendency for convective fluid flow to develop is inversely related to the product of G and R. Using this and other relationships involving G and R, various macroscopic criteria were developed from experimental data and used to predict the formation of grain defects.[1,7,16,17] In addition, recent solidification modeling efforts have also focused on predicting freckle formation and the role of solute in the breakdown of single-crystal solidification.[8,12,13,18]

Preventing the formation of grain defects during solidification becomes more complicated when dealing with noncylindrical castings. Rapid transitions in geometry, such as those seen in blade-shaped components, can often result in the curvature of the liquidus isotherm that leads to thermal undercooling and/or localized changes in the solidification parameters.[14,19] In single-crystal alloys that exhibit a low undercooling capacity, the undercooling may result in the formation of structural inhomogeneities such as misoriented grains. Although the macroscopic criteria for predicting grain-defect formation assume uniform thermal gradients, transitions in geometry may result in localized changes of the solidification parameters, which can potentially initiate convective fluid flow and lead to freckle formation.[14] Currently, through solidification modeling, mold-withdrawal profiles can be optimized to a certain degree to prevent the formation of defects due to component geometry.[11–14,19,20]

For nominally constant casting-geometry and processing conditions, it has been previously shown that increasing the level of tantalum and reducing the levels of rhenium and/or tungsten in the alloy minimizes the onset of freckling

S. TIN, Graduate Research Associate, and T.M. POLLOCK, Professor, are with the Department of Materials Science and Engineering, University of Michigan, Ann Arbor, MI 48109. W. MURPHY, Senior Engineer, is with General Electric Aircraft Engines, Cincinnati, OH 45215.

Manuscript submitted June 27, 2000.

under conditions where relatively low thermal gradients are present.[2,3] During directional solidification, the progressive depletion of the high-density refractory constituents (tungsten and rhenium) in the segregated solute creates a density inversion in the mushy zone. Tantalum, which has the opposite partitioning behavior, segregates preferentially to the interdendritic solute and offsets the depletion of tungsten and rhenium, subsequently decreasing the driving force for convection.[3,21] Although freckles and misoriented grains can potentially be reduced by optimizing the levels of tantalum, tungsten, and rhenium, this is unlikely to simultaneously benefit the phase-stability, corrosion, creep, and fatigue properties. Therefore, alloying alternatives that improve solidification characteristics without significantly compromising the physical and mechanical properties of the alloy are highly desirable.

Carbon additions to equiaxed and directionally solidified (DS) superalloys were originally intended to strengthen grain boundaries through the formation of various MC carbides.[22,23] With the development of single-crystal components, grain-boundary strengthening elements such as Hf, B, C, and Zr were eliminated or intentionally kept at low levels in an attempt to increase incipient melting temperatures and permit complete solutioning of the γ' phase.[22–25] Recently, minor additions of carbon have been reintroduced to a number of commercial Ni-based single-crystal alloys to improve the mechanical properties transverse to low-angle grain boundaries that are often present in single-crystal components.[26,27]

In this study, the effect of carbon additions on grain-defect formation during solidification was studied in high-refractory single-crystal alloys with relatively large variations in the levels of tantalum, tungsten, and rhenium. Of particular interest was the influence of carbon additions on the segregation behavior of the constituent elements and the relationship between MC carbide precipitation and the tendency to form freckle defects. Results from detailed analyses of segregation, characterization of carbides, and differential thermal analyses on a large number of carbon-containing experimental single-crystal alloys are reported and compared to similar alloys with no intentional carbon additions. Based on these observations, a brief discussion regarding the potential influence of carbon in solution and carbide precipitation on the processes involved in freckle formation follows.

II. EXPERIMENTAL MATERIALS AND PROCEDURE

Twenty-three experimental single-crystal alloys with variable levels of alloying additions were selected as part of an experimental program designed to investigate the influence of alloy chemistry on the breakdown of single-crystal solidification. Levels of interstitial impurities were kept constant through the use of a solute-lean master heat, which was sectioned, remelted, and doped to generate the compositions listed in Table I. Except for the segregation analyses, results from the series of alloys containing no intentional carbon additions have been previously reported by Pollock *et al.*[2] and are included for comparative purposes.

A production-scale Bridgman furnace was used to simultaneously solidify seven solid blade-shaped castings of each alloy composition in a ceramic cluster mold under approximately constant solidification conditions. Schematics of the furnace and mold configurations were also reported earlier.[2] In all cases, solidification of the single-crystal alloys occurred under fixed processing conditions, consisting of a thermal gradient of approximately 10 °C/cm at the growth front and a constant withdrawal rate of 40 cm/h.

Table I. Nominal Compositions of Experimental Single-Crystal Alloys (Wt Pct)

Alloy	Al	Cr	Co	Hf	Re	Ta	W	Mo	C	Ni
SX-1	6.0	4.5	12.5	0.16	6.3	7.0	5.8	0.0	0.05	bal
SX-2	6.1	4.5	12.5	0.15	6.5	9.0	5.8	0.0	—	bal
SX-3	5.7	4.0	11.5	0.12	5.0	6.0	5.0	0.0	—	bal
SX-4	5.7	5.0	13.5	0.12	5.0	6.0	6.5	0.5	—	bal
SX-5	6.3	4.0	13.5	0.18	6.5	6.0	5.0	0.0	—	bal
SX-6	6.3	5.0	11.5	0.18	6.5	6.0	6.5	0.5	—	bal
SX-7	6.3	5.0	11.5	0.12	5.0	9.0	5.0	0.0	—	bal
SX-8	6.3	4.0	13.5	0.12	5.0	9.0	6.5	0.5	—	bal
SX-9	5.7	5.0	13.5	0.18	6.5	9.0	5.0	0.0	—	bal
SX-10	5.7	4.0	11.5	0.18	6.5	9.0	6.5	0.5	—	bal
SX-11	6.1	4.5	12.5	0.15	5.0	9.0	5.8	0.0	0.1	bal
SX-12	6.1	4.5	12.5	0.15	6.5	9.0	5.8	0.0	0.1	bal
SX-13	6.3	5.0	13.5	0.18	5.0	6.0	5.0	0.5	0.1	bal
SX-14	6.3	4.0	11.5	0.18	5.0	6.0	6.5	0.0	0.1	bal
SX-15	5.7	5.0	11.5	0.12	6.5	6.0	5.0	0.5	0.1	bal
SX-16	5.7	4.0	13.5	0.12	6.5	6.0	6.5	0.0	0.1	bal
SX-17	5.7	4.0	13.5	0.18	5.0	9.0	5.0	0.5	0.1	bal
SX-18	5.7	5.0	11.5	0.18	5.0	9.0	6.5	0.0	0.1	bal
SX-19	6.3	4.0	11.5	0.12	6.5	9.0	5.0	0.5	0.1	bal
SX-20	6.3	5.0	13.5	0.12	6.5	9.0	6.5	0.0	0.1	bal
SX-21	6.0	4.5	12.5	0.13	6.1	7.8	5.8	0.0	0.05	bal
SX-22	6.0	4.5	12.5	0.13	6.2	8.4	5.8	0.0	0.05	bal
SX-23	6.0	4.5	12.5	0.15	6.8	6.8	6.0	0.0	0.04	bal

As-cast crystals were etched to assess the number, type, and location of freckles and misoriented grains. Following this, castings were sectioned for analyses of carbide morphology and composition, segregation characteristics, and phase transformations. Carbides were extracted from the as-cast alloys containing intentional carbon additions using an electrolytic process.[28] With a platinum sheet acting as the cathode, small rectangular samples (~5 g) were sectioned from the dovetail region of the casting, polished, and charged with ~0.04 A/cm^2 in a solution of 9:1 HCl:methanol + 1 wt pct tartaric acid for 8 to 10 hours to dissolve the γ-γ' matrix. The resulting carbides were then collected and placed in a Rigaku X-ray Diffractometer (XRD) for lattice parameter measurements. A PHILIPS* XL30 FEG scanning electron microscope (SEM) equipped with an Oxford energy-dispersive spectroscopy (EDS) system was used to characterize the carbide morphologies and perform qualitative EDS measurements on the carbides.

*PHILIPS is a trademark of Philips Electronic Instruments Corp., Mahwah, NJ.

A two-step process was used to characterize segregation and to subsequently assess distribution coefficients (k) *via* a Scheil-type analysis. This technique is similar to the ranking technique reported by Gungor[29], Huang, *et al.*[30] and Nastac.[31] As-cast samples were first sectioned normal to the ⟨001⟩ growth direction. Next, an EDS line scan that traversed the primary dendrite core into the interdendritic region was used to determine whether individual elements

segregate to the dendrite core or the interdendritic region. A second series of analyses were then conducted to measure the composition at points in a square grid composed of 225 points. The grid was placed over a representative section of the dendritic microstructure, covering ~1.2 mm^2. The composition data acquired for the individual elements were then ranked according to their characteristic segregation behavior. For elements having distribution coefficients greater than 1, as determined previously by the line scan, the composition data were ranked in descending order and plotted on an apparent-fraction solid scale, yielding a Scheil plot. Composition data for elements segregating to the interdendritic regions were ranked in ascending order and plotted in the same manner. Distribution coefficients were then extracted by fitting the plots with a Scheil equation[2] and/or a modified Scheil analysis,[3] which accounts for back-diffusion.

$$C_s = kC_0(1 - f_s)^{k-1} \quad [2]$$

$$C_s = kC_0(1 - (1 - 2\alpha k)f_s)^{k-1/1-2\alpha k} \quad [3]$$

where C_s is the local composition of the solid, C_0 is the nominal alloy composition, α is the Fourier number, and f_s is the fraction of solid. This analysis assumes that the data collected were representative of the entire sample and that the distribution coefficients were constant. Steps were taken to determine the validity of these assumptions. First, the mean composition from the EDS point measurements was compared to the actual compositions of the different samples measured using X-ray fluorescence (XRF). Experimental Scheil plots generated from the point measurements were also compared to theoretical Scheil plots with constant k values, to detect any deviations between the two curves. Quantitative composition measurements have been carried out on a PHILIPS XL30 FEG SEM equipped with the Oxford EDS system.

Finally, a SETARAM SETSYS 18 differential thermal analysis (DTA) unit was used to investigate the effects of alloying composition on alloy solidus, liquidus, and carbide precipitation temperatures. Prior to testing of the experimental alloys, the DTA unit was calibrated with high-purity Ni (99.99 + pct) and Ag (99.9999 pct) at scanning rates of 3 °C/min, 5 °C/min, 10 °C/min, and 20 °C/min using a platinum reference. All tests were conducted in a purged ultrahigh-purity argon atmosphere (flow rate ~70 cc/min) using high-purity alumina crucibles. Once calibrated, cylindrical samples (4 mm in diameter and ~3 to 4 mm in height) with masses ranging from 200 to 250 mg were prepared from the various alloys. Since the samples prepared for DTA were relatively large and had a diameter of approximately 10 times the characteristic segregation length (the PDAS), it could be assumed that the analysis was representative of the entire alloy. Due to the effects of undercooling, only the DTA traces collected during heating were evaluated. The heating cycle of the samples consisted of

(1) room temperature to 1000 °C at 20 °C/min,
(2) 10-minute isothermal soak at 1000 °C, then
(3) 1000 °C to 1550 °C at 5 °C/min.

For this particular application, a scanning rate of 5 °C/min was determined to yield the best combination of temperature accuracy and peak resolution. Following the DTA experiments, the samples were metallographically prepared and examined to ensure that no major contamination or interaction with the alumina crucibles occurred during the analyses.

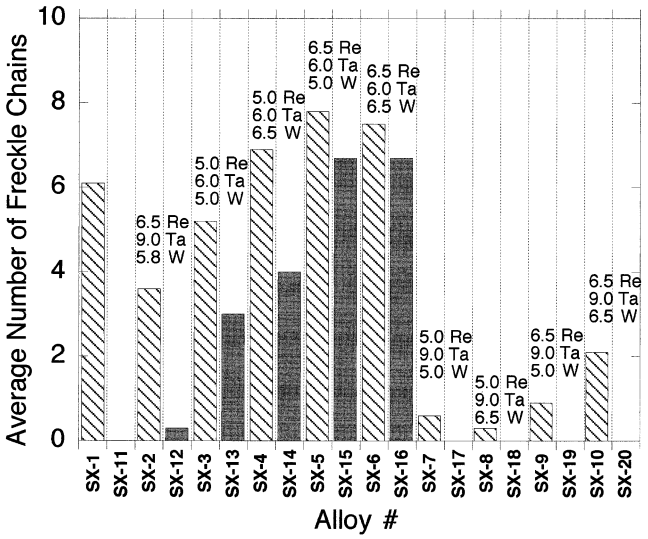

Fig. 1—The influence of alloy chemistry on the number of freckle chains for constant solidification conditions. Columns representing the noncarbon containing alloys are striped and the corresponding columns for the carbon containing alloys are shaded gray.

III. RESULTS

Figure 1 summarizes the results of solidification experiments on alloys SX-1 through SX-20. Under constant processing conditions, carbon additions of 0.1 wt pct to the experimental alloys had a strong beneficial influence on the average number of freckle chains observed on single crystals solidified in investment cluster molds. Previous investigations have shown that while levels of Re, W, and Ta strongly influence grain-defect formation, no statistically significant effects were measured with similar variations in Al, Cr, Co, Hf, and Mo levels.[2] Consequently, for fixed levels of Re, W, and Ta, carbon additions of 0.1 wt pct reduced the number of freckle defects for all alloys investigated. Upon closer examination of the results, however, the effectiveness of the carbon additions in reducing freckle defects did vary from alloy to alloy. For example, substantial improvements in the solidification characteristics were observed in alloys SX-12 and SX-20, while only minor improvements occurred in alloys SX-15 and SX-16. Alloys containing elevated levels of tantalum in conjunction with the intentional carbon additions were least prone to the formation of freckle defects (alloys SX-17 through SX-20). Neither the dendrite morphology nor the development of secondary and tertiary dendrite arms in the as-cast alloys was affected by additions of carbon (Figure 2). To better understand the mechanism(s) by which carbon influences the solidification process, crystals of each of these alloys were further analyzed in detail in their as-cast form.

A. *Carbides*

With the addition of 0.1 wt pct carbon to the experimental alloys, a small volume fraction of MC carbides (where "M" indicates metallic elements) formed during solidification.

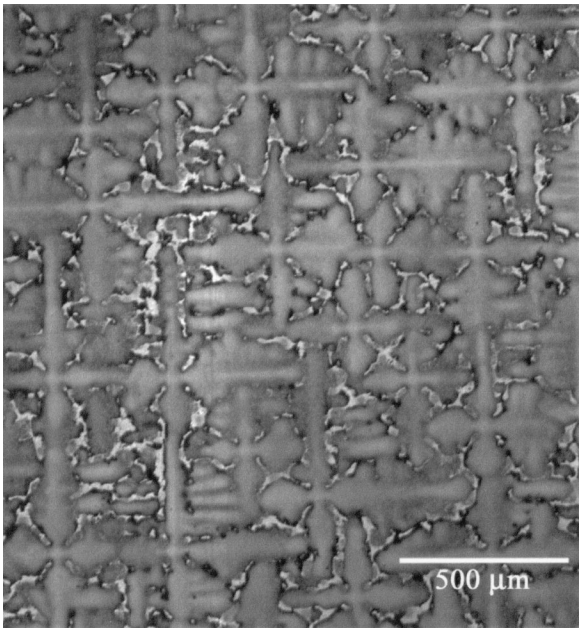

(*a*)

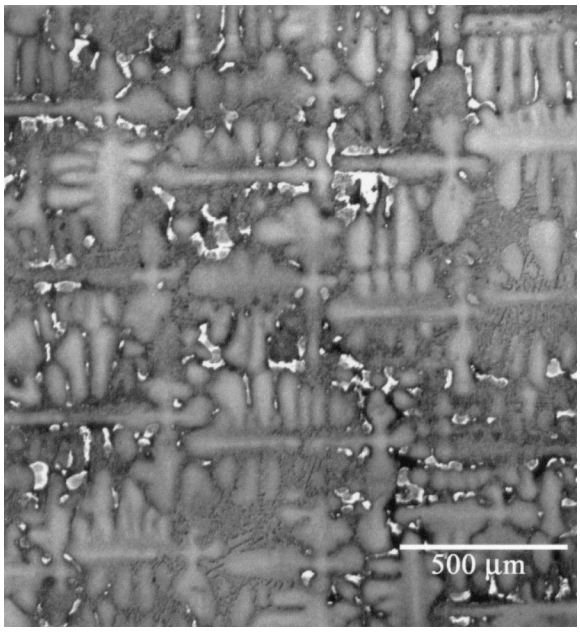

(*b*)

Fig. 2—Optical photomicrographs of the as-cast dendritic microstructure present in the dovetail region of specimen (*a*) SX-2 and (*b*) SX-12. Note the significant development of secondary and tertiary dendrite arms under the imposed solidification conditions (R = 40 cm/h, and G = ~10 °C/cm).

Using a digital image-analysis technique, the volume fraction of the carbides was measured to be approximately 1 to 2 pct. Optical microscopy on metallographically prepared as-cast specimens revealed that all carbides were preferentially located in the interdendritic regions surrounded by a γ-γ' matrix. Three different carbide morphologies were observed: blocky, script, and nodular. Examples of these three morphologies are shown in Figures 3 through 5, respectively, in samples that were subjected to electrolytic etching for long periods of time to remove the surrounding nickel material.

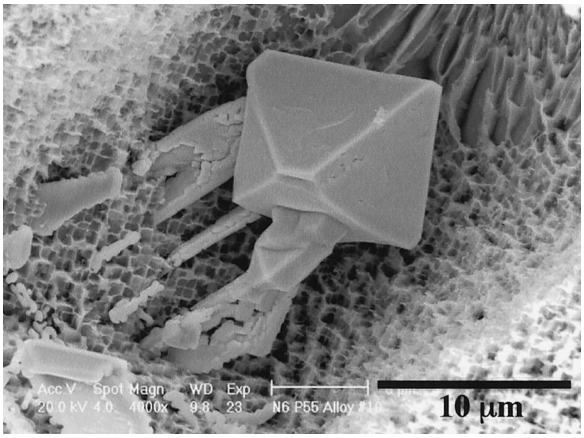

Fig. 3—SEM micrograph of a blocky Ta-rich carbide with lamellar growth extensions in a deeply etched sample.

The EDS analyses indicated that these carbides consist primarily of Ta with small amounts of Ni, Hf, Co, Cr, and Mo. Stoichiometric TaC has a lattice parameter of 4.4547 Å, a density of 14.5 g/cm^3, and a cubic NaCl-type crystal structure. Lattice parameters of the extracted carbides were influenced by the presence of minor amounts of Ni, Hf, Co, Cr, and Mo and varied from 4.430 to 4.448 Å (Table II).

Blocky carbides made up a very small fraction of the carbides present in the microstructure of the various samples. Their characteristic blocky, faceted shape was revealed only after the surrounding γ-γ' matrix was etched away (Figure 3). These carbides were typically very large (>10 μm), occasionally had lamellar growth extensions, and had no detectable orientation relationship with the surrounding nickel crystal.

Script carbides were more commonly observed than blocky carbides. Careful extraction of these carbides revealed large, lacy, interconnected structures composed of rods or sheets (Figure 4). The Chinese script-like morphologies that were observed on polished samples were actually cross sections of these large lacy structures. Interestingly, a strong orientation relationship existed between the radial [100] and [010] dendrite growth directions and the script carbides. The rods or sheets that comprise the lacy structure were all oriented parallel to the [100] or [010] dendrites.

The third carbide morphology identified in these Ni-based superalloys consisted of carbide rods and sheets with submicron nodules uniformly spaced all along the surfaces (Figure 5). Unlike the script carbides, the orientation of these "nodular" carbides was not restricted to the ⟨010⟩ directions. The majority of the carbides examined from alloys SX-11 through SX-23 were either of the nodular or script morphology. An interesting observation regarding the nodular carbides was their preferential presence at the edges of castings. This may indicate that trace elements such as Si, N, and O influence carbide morphology, since these elements would be present in slightly enhanced quantities in near-surface regions of the castings, due to the use of investment molds. In most of the alloys with carbon additions, carbides of all three morphologies were observed throughout the entire length of the blade-shaped casting in both the airfoil and dovetail regions. On average, corresponding PDAS measurements taken from the airfoil and dovetail region of the castings were ~410 and ~450 μm, respectively. Thus, the slight

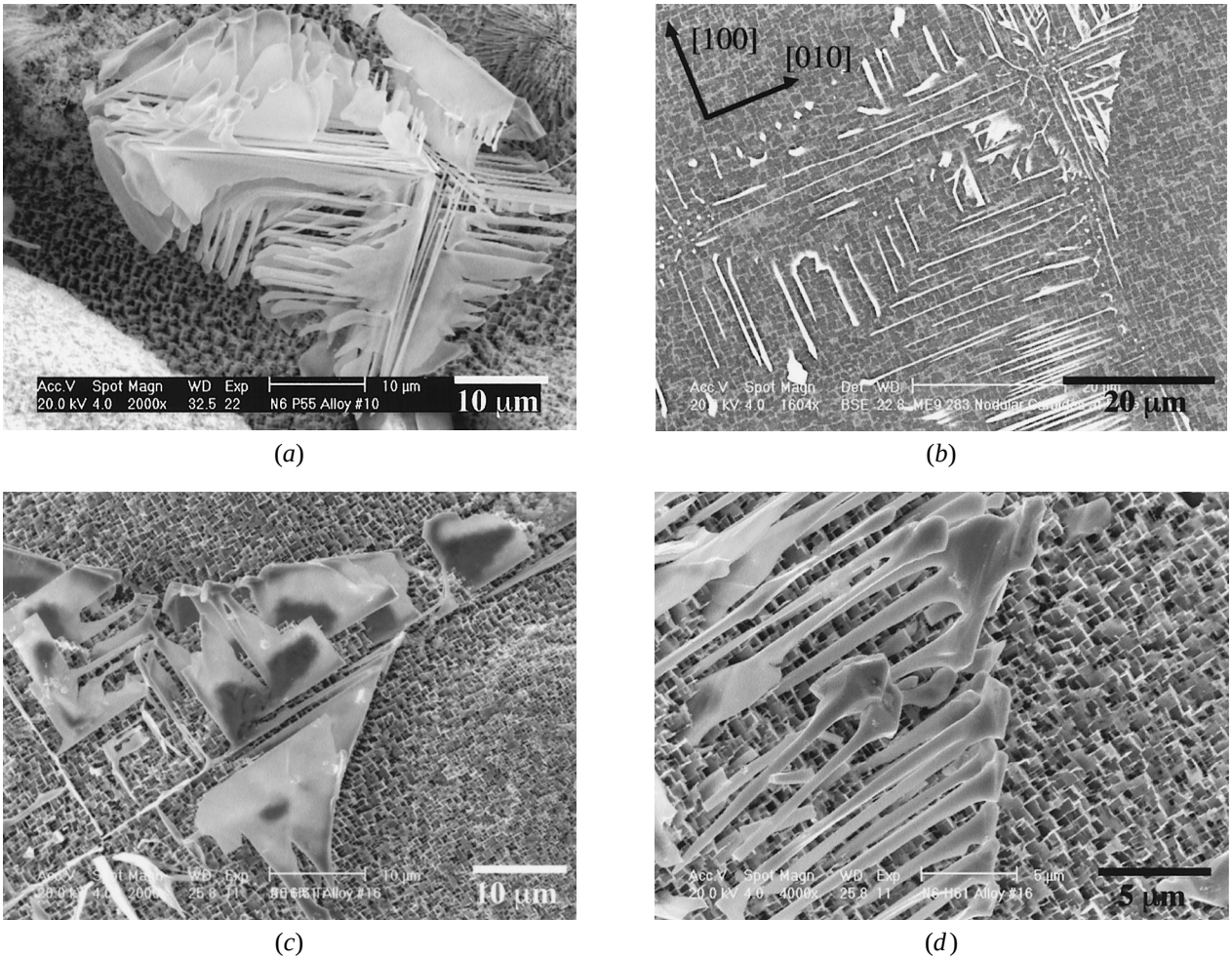

(*a*) (*b*)

(*c*) (*d*)

Fig. 4—(*a*) SEM micrograph of a lacy script carbide revealing an interconnected structure composed of rods and sheets. (*b*) Back-scattered SEM micrograph of a polished cross section showing the orientation dependence of script carbides found in the interdendritic regions with the radial dendrite growth directions. (*c*) SEM micrograph of a lacy carbide sheet. (*d*) SEM micrograph of script carbide rods.

difference in thermal gradients between the airfoil and dovetail region of the castings during solidification did not significantly affect the development of these carbide morphologies.

The blocky carbides, which apparently form at the highest temperature, had little to no solubility for elements other than tantalum and hafnium. However, small amounts of Ni, Co, Cr, and, occasionally, Mo were detected in the script and nodular carbides. In some instances, the carbides observed within the castings were completely nodular or script types, indicating that overall alloy chemistry is also important to carbide morphology. Table II lists the majority carbide morphology (consisting of >75 vol pct) identified for each of the alloys investigated. In spite of the variation in morphology and composition of the carbides, no correlation was found between carbide morphology and/or chemistry and the tendency to form freckles within this set of alloys. Metallographic examination and serial sectioning of the as-cast specimens revealed no instances of grain nucleation at the carbides.

B. *Segregation Characteristics*

Because carbon additions and/or carbide formation in the mushy zone during solidification could potentially result in qualitative changes in the solidification path, the segregation characteristics of constituent elements in carbon-containing and comparable carbon-free alloys were studied in the as-cast crystals.

Quantitative EDS measurements across the primary dendrites normal to the [001] growth direction revealed that Ta, Al, and Ni segregate preferentially to the interdendritic regions while Re, W, Co, Cr, and Mo segregate to the dendrite core (Figure 6). To validate the major assumptions made in the two-step Scheil analysis described earlier, the mean composition calculated from the EDS point measurements from representative samples was compared to compositions determined by XRF in Table III. The differences between the two sets of composition data are negligible, indicating that the area being sampled was representative of the entire specimen. Comparison of the experimental data and the fitted Scheil analysis for Ta in alloy SX-12 (Figure 7) shows good agreement, except in the very early stages of solidification (within the first few percentages of fraction of solid). Similarly good agreement was found for all other constituent elements, indicating that the assumption of a constant k value was reasonable. When determining distribution coefficients using this method, k and α values were weighted such that the best fit between the experimental and

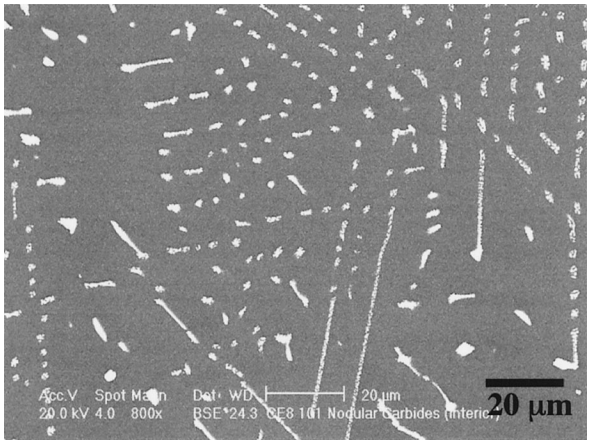

(*a*)

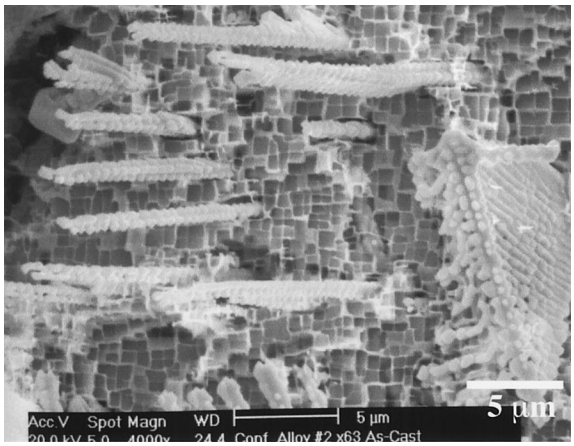

(*b*)

Fig. 5—(*a*) Back scattered SEM micrograph of nodular carbides present in the interdendritic regions of a polished cross section. (*b*) SEM micrograph of nodular carbides present in the forms of rods and sheets.

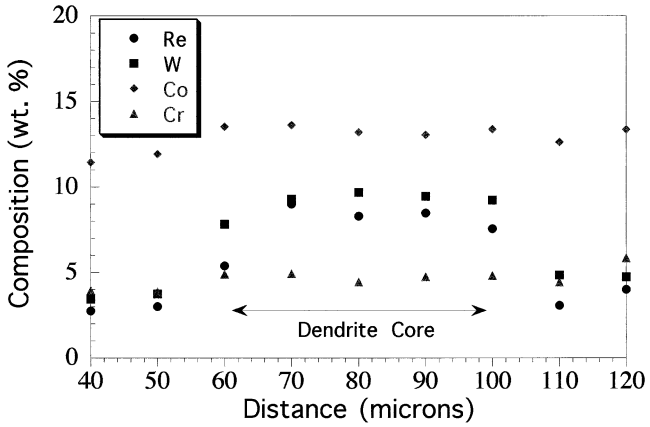

(*a*)

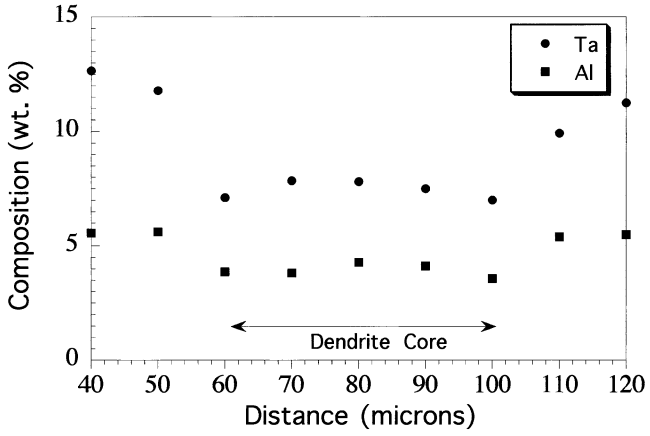

(*b*)

Fig. 6—Linescan of SX-11 across the primary dendrite core showing the elements segregating (*a*) to the dendrite core and (*b*) to the interdendritic regions.

Table II. Carbide Morphology and Lattice Parameter Measurements for Experimental Alloys

Alloy	Majority Carbide Morphology	Lattice Parameter, Å
SX-11	script	4.440
SX-12	mixed	4.434
SX-13	nodular	4.441
SX-14	script	4.440
SX-15	nodular	4.446
SX-16	nodular	4.441
SX-17	nodular	4.442
SX-18	nodular	4.443
SX-19	nodular	4.441
SX-20	mixed	4.430
SX-22	script	4.448
SX-23	nodular	4.444

*Majority carbide morphology is defined as the morphology that makes >75 pct of the carbides.

Scheil analyses occurred in the region where the apparent fraction of solid ranged from ~0.3 to 1.0. Table IV lists the distribution coefficients for all constituent elements in a number of carbon-containing and carbon-free experimental single-crystal alloys. Significant deviations between the experimental ranked distribution data and Scheil analyses were observed with small changes in k (Figure 7); hence, the precision of this method falls within an estimated ±0.05 of the values reported in Table IV.

Due to the volume of material sampled by the electron beam during the EDS analysis, certain sources of error need to be addressed when using the Scheil-fitting method of determining equilibrium distribution coefficients. Since the electron beam is providing an average composition for a finite volume of material sampled, this does not accurately predict the segregation behavior in the initial and final stages of solidification. Figure 7 clearly shows a deviation between the experimental data and the fitted Scheil curve during the initial stages of solidification. The deviation in the final stages of solidification, however, is minimized when back-diffusion is taken into consideration. Nevertheless, this method is effective in revealing trends and differences in segregation behavior among this set of alloys.

Figure 8 shows a comparison of the tantalum distribution curves for two nominally identical alloys with and without carbon additions (alloy SX-12 contains carbon). The data show that for both alloys, tantalum segregation to the interdendritic region occurs in a very similar manner up until

Table III. Representative Comparison of Chemistries for Segregation Analysis (Wt Pct)

Element	SX-9	Mean EDS	SX-19	Mean EDS	SX-6	Mean EDS	SX-16	Mean EDS
Al	5.75	5.99	6.20	6.47	6.20	6.23	5.70	5.96
Cr	4.60	4.81	3.70	3.80	4.60	4.80	3.74	3.87
Co	13.10	13.38	11.20	11.44	11.15	11.41	13.20	13.41
Ni	55.50	54.68	56.80	55.94	57.70	58.05	57.50	56.35
Ta	9.10	9.22	9.00	9.20	6.35	6.17	6.17	6.27
W	5.05	5.21	5.05	5.56	6.50	6.59	6.45	7.15
Re	6.40	6.60	6.50	7.25	6.30	6.32	6.50	6.83
Y	—	—	0.1	—	—	—	0.11	—
Mo	0.04	—	0.55	0.48	0.55	0.50	0.03	—
Hf	0.17	—	0.1	—	0.17	—	0.1	—
C	0.00	—	0.1	—	0.00	—	0.1	—

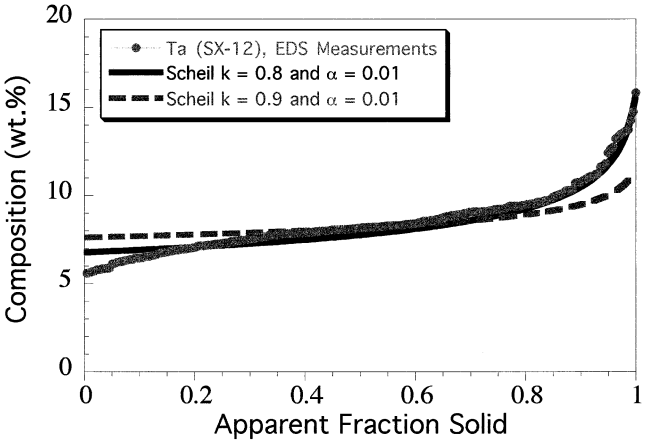

Fig. 7—Comparison of experimental data and theoretical Scheil curves for Ta in SX-12. Theoretical Scheil curves were plotted, accounting for limited back diffusion with Eq. [2], using distribution coefficients of 0.8 and 0.9 for Ta and a Fourier number (α) of 0.01. Slight variations in k result in significant changes in the slope of the Scheil curve.

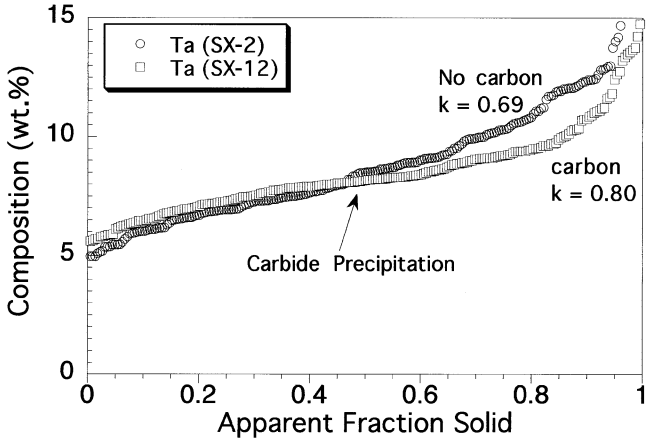

Fig. 8—Comparison of the Ta distribution for nominally similar alloys with and without carbon additions. Separation of the curves indicates formation of TaC in the mushy zone at ~0.5 fraction solid in alloy SX-12.

approximately a 0.5 apparent fraction of solid. Separation of the curves at this point indicates a change in the segregation behavior due to carbon. The difference in the overall slope of the two curves is captured by the fitted distribution coefficients for the two alloys. In the case of the carbon-containing alloy (SX-12), the value of k is obviously an average which represents the segregation behavior both before and after carbide precipitation. The fitted distribution coefficients for alloys SX-2 and SX-12, respectively, are 0.69 and 0.80. In both cases, a Fourier number of 0.01 was used to account for the limited back-diffusion taking place during solidification. Referring to the results shown in Table IV, the carbon additions result in less segregation of the refractory constituents which are known to affect freckling, including W, Re, and Ta. Figure 9 reveals the differences in the distribution of W in alloys SX-2 and SX-12. Interestingly, despite the absence of W in the carbides, the segregation behavior of W was significantly affected by the carbon addition. In alloys SX-6 and SX-16, where the beneficial effect of carbon on freckle formation is less pronounced, a smaller change in the partitioning behavior of W and Re was measured in the alloy with the carbon addition. Finally, comparison of the distribution

Table IV. Distribution Coefficients for Experimental Alloys

Element	SX-2	SX-12	SX-3	SX-13	SX-6	SX-16	SX-9	SX-19	SX-10	SX-20
Al	0.81	0.86	0.89	0.88	0.87	0.90	0.87	0.88	0.84	0.87
Cr	1.16	1.13	1.08	1.05	1.07	1.06	1.12	1.12	1.17	1.13
Co	1.08	1.13	1.05	1.05	1.07	1.03	1.07	1.06	1.10	1.08
Ni	0.94	0.95	0.95	0.96	0.95	0.95	0.95	0.95	0.94	0.93
Ta	0.69	0.80	0.79	0.88	0.80	0.89	0.77	0.83	0.74	0.76
W	1.54	1.38	1.54	1.39	1.42	1.36	1.54	1.44	1.42	1.39
Re	1.60	1.49	1.43	1.42	1.38	1.33	1.43	1.36	1.41	1.41
Mo	—	—	—	1.46	1.40	—	—	1.35	—	—

*Distribution coefficients were determined by fitting the modified Scheil analysis, which accounts for back diffusion to the experimental data. In all cases, $\alpha = 0.01$. The estimated precision of the average fitted k values was determined to be approximately ± 0.05.

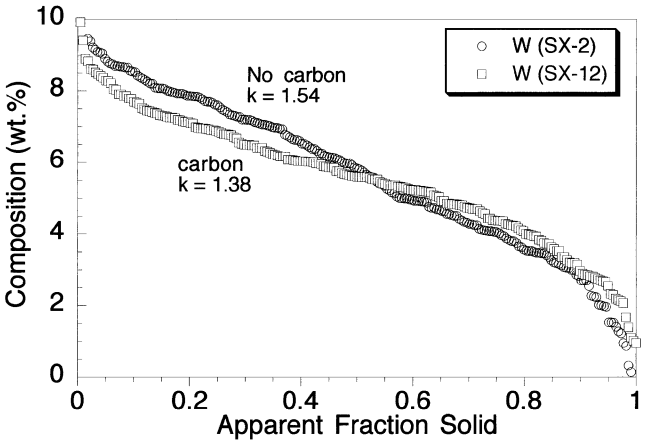

Fig. 9—Comparison of W distribution for nominally similar alloys with and without carbon additions. Although no W was detected in the carbides, the segregation behavior of W was altered by the carbon addition.

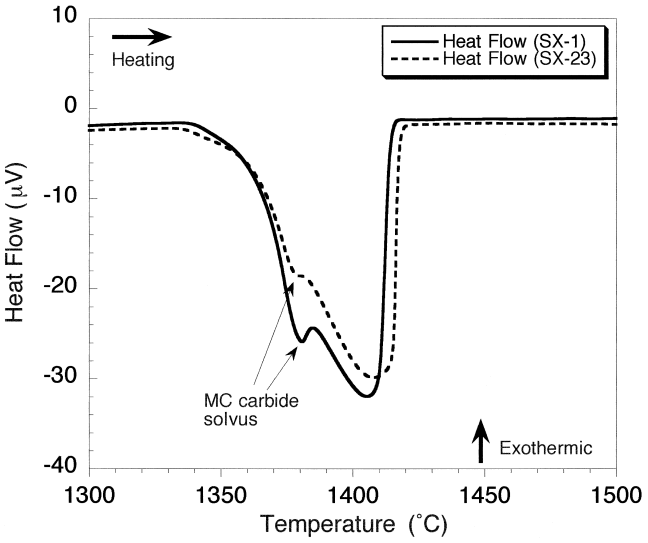

Fig. 10—DTA traces from nominally similar alloys SX-1 and SX-23.

coefficients for Al, Cr, Co, and Ni in Table IV reveals similar behavior for comparative carbon–carbon-free alloys.

C. *Differential Thermal Analysis*

DTA of the as-cast experimental single crystals revealed information on the effects of alloy composition on the solidus liquidus and carbide precipitation temperatures. Figure 10 shows the results for alloys SX-1 and SX-23, which are quite close to one another in composition. Note for both alloys the presence of an MC carbide peak just below the liquidus temperature. This is consistent with the segregation data (Figure 8), which also indicate that the precipitation of the carbides occurs just below the liquidus temperature. The traces for these two alloys are very similar in appearance, except that the higher level of carbon in SX-1 results in a more pronounced carbide peak occurring at ~1385 °C, and the slightly higher levels of Re and W in alloy SX-23 apparently result in a modest increase in the liquidus temperature.

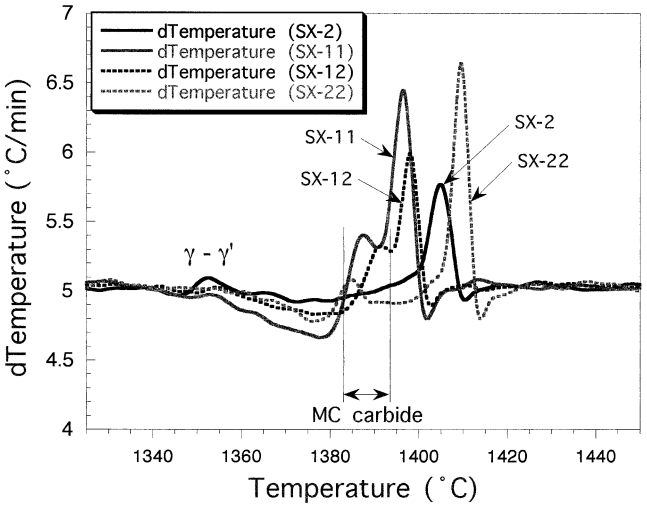

Fig. 11—Differences observed in the DTA traces of alloys SX-2, SX-11, SX-12, and SX-22 illustrate the effects of composition on liquidus, solidus, and carbide precipitation temperatures.

Table V. Liquidus, Solidus, and Carbide Precipitation Temperature Measurements for Experimental Alloys with Carbon

Alloy	T_L, Liquidus* (°C)	T_S, Solidus* (°C)	T_C, Carbide Precipitation** (°C)
SX-11	1396	1360	1386
SX-12	1399	1358	1390
SX-13	1398	1361	1383
SX-14	1409	1367	1391
SX-15	1408	1366	1389
SX-16	1413	1371	1391
SX-17	1397	1364	1386
SX-18	1393	1358	1386
SX-19	1388	1350	1386
SX-20	1383	1342	1377
SX-22	1411	1363	1383
SX-23	1415	1360	1381

*Liquidus and solidus temperatures are reported from integrated heat flow curves.

**Carbide dissolution temperatures are reported from *d* Temperature curves.

Results from the DTA shown in Figure 11 further reveal the effect of alloying additions on the liquidus and MC carbide precipitation temperatures. Alloys SX-2 and SX-12 are nominally the same composition, with the only difference being the addition of ~0.1 wt pct carbon to alloy SX-12. Compared to alloy SX-2, carbon lowers the liquidus temperature in alloy SX-12 by 6 °C and results in a carbide dissolution reaction occurring in the mushy zone at ~9 °C below the liquidus temperature. The DTA traces of alloys SX-11 and SX-22, respectively, suggest that the rhenium additions slightly increase the liquidus, while aluminum additions reduce liquidus temperatures. In addition, the less pronounced endothermic MC carbide peak observed in alloy SX-22 is most likely due to the lower carbon content in the alloy. Collective results of the DTA analyses (Table V) indicate that the MC carbide dissolution temperatures (1377

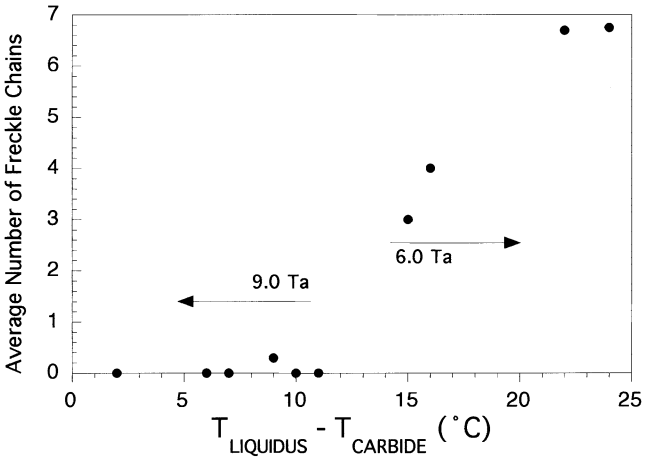

Fig. 12—Plot of relative carbide precipitation *vs* average number of freckle chains. Permeability of the mushy zone would be influenced most by carbides that precipitate closest to the liquidus.

°C to 1391 °C) are much less sensitive to shifts in composition, compared to the solidus (1342 °C to 1371 °C) or liquidus (1383 °C to 1415 °C) temperatures, within this set of experimental alloys. Based on these results fewer freckle defects were associated with alloys in which carbide dissolution temperatures approached those of the liquidus, Figure 12.

IV. DISCUSSION

Over the range of compositions investigated in these high-refractory nickel-based single crystals, carbon additions are beneficial in reducing the number of freckle defects that form during solidification. While it is well known that carbon additions result in the formation of Ta-rich MC carbides, the freckle-generating mechanisms affected by the carbides have not yet been investigated. Considering Eq. [1], a number of potential interactions could be responsible for the reduced tendency for initiation of thermosolutal convective instabilities. (1) Carbon additions alter the segregation behavior of the constituent elements and/or the solidification path of the alloy. (2) The precipitation, growth, and coalescence of refractory carbides, which have a density higher than that of the surrounding liquid, affects the viscosity and local fluid-flow patterns associated with thermosolutal convective instabilities. (3) Carbide precipitation in the mushy zone during solidification lowers the permeability of the dendritic network. (4) Carbide networks that develop within the interdendritic regions of the mushy zone inhibit the dendrite fragmentation process and suppress the transport of dendrite fragments that subsequently lead to the formation of grain defects.

Results from this study reveal that the segregation behavior of the constituent refractory additions in the single-crystal alloys were affected by the precipitation of nodular and/or script carbides in the mushy zone. Distribution coefficients for a number of nominally similar alloys with and without intentional carbon additions were measured using a Scheil-type analysis. In general, the coefficients determined in this study did not vary significantly from those reported in the literature for similar alloys.[30,32] The abrupt separation of the tantalum distribution curves (Figure 6) was observed in all comparative carbon-containing and carbon-free alloys, regardless of the resultant carbide morphology. After separation, the tantalum distribution curves for the carbon-containing alloys were 1 to 2 wt pct lower than their carbon-free counterparts. The 1 to 2 wt pct (~0.5 at. pct) deviation was consistent with the TaC reaction, consuming the 0.1 wt pct (~0.5 at. pct) carbon in solution.

It is interesting that the precipitation of Ta-rich MC carbides is beneficial, since it would deplete tantalum from the liquid in the mushy zone. In alloys with no carbon, the enrichment of tantalum in the liquid is beneficial with respect to stabilizing against convective instabilities, as exhibited by a comparison of the results from alloys SX-7 through SX-10 in Figure 1. However, the reduced distribution coefficients for tungsten and rhenium in the carbon-containing alloys indicate that comparatively higher levels of these high-density refractory elements were present in the liquid phase of the mushy zone during solidification. The Navier–Stokes equation for the upward buoyancy force (f_z) due to thermal and solutal gradients during unidirectional solidification is[33]

$$f_z = -g\rho(\beta_T(T - T^*) + \beta_C(C - C^*) \qquad [4]$$

where

$$\beta_T = -(\partial \ln \rho/dT)_C \qquad [5]$$

$$\beta_C = -(\partial \ln \rho/dC)_T \qquad [6]$$

and T^* and C^* are the average temperature and concentration, respectively, and g is the gravitational constant. This indicates that convection occurs when the temperature and concentration-density gradients exceed some critical value. Liquid densities are known to vary as a function of refractory-element content. However, for complicated multicomponent alloy systems, liquid densities can only be quantitatively estimated.[34,35] Based on the liquid-density data from a similar alloy[34] (PWA 1484), it is expected that increasing the concentration of tungsten and rhenium in the segregated solute lowers the density gradient between the solute and the bulk liquid during solidification. Hence, the driving force for the convective fluid flow which subsequently leads to the formation of grain defects can be decreased by minimizing the extent of tungsten and rhenium segregation during solidification.

The measured carbide dissolution temperatures are insensitive to minor changes in alloy chemistry and variations in carbide morphology. Except in alloy SX-20, where the liquidus temperature is 1383 °C, DTA data reveal that carbide dissolution for these experimental alloys occurs at ~1386 °C. This temperature is very close to that of the proposed trough (~1380 °C) in the nickel-rich region of the Ni-Ta-C ternary system, which leads to the formation of γ/TaC/Ni_3Ta.[36] Depending on the levels of other alloying constituents, dissolution of nodular and/or script carbides may be occurring anywhere from 2 °C to 34 °C below the liquidus temperature of the alloy, as estimated in the present DTA apparatus. Although there were variations in the bulk-alloy chemistry, the compositions of the script and nodular carbides remained relatively unchanged, as revealed by EDS measurements and their lattice parameters. The uniformity of the nodule spacing on the surfaces of these lamellar nodular carbides and their lack of orientation dependence suggests that the solidification path of the alloy may have been altered by a final TaC/γ eutectic reaction. A similar MC/γ reaction

has been reported by Willis in directionally solidified and quenched MAR-M002[37] and by Fras in directionally solidified NiTaC composites.[38] Intricate script carbides, on the other hand, apparently have their growth directions constrained by the surrounding ⟨001⟩ dendrites.[39,40,41] It has been well documented that eutectic microstructures are sensitive to local solidification conditions[42] and can vary significantly in multicomponent alloys. Although the script and nodular carbides differ in appearance, no relationship between the resulting carbide morphology in the as-cast samples and the measured distribution coefficients could be determined. Relative to comparable alloys without intentional carbon additions, less segregation of Re, W, and Ta was measured in as-cast alloys that contained carbides, regardless of morphology.

Blocky carbides with their faceted features, however, are indicative of microstructures formed in the liquid, where near-equilibrium growth is possible. With the density of TaC being almost twice that of the Ni-based alloy near its liquidus temperature, it would be reasonable to assume that if the blocky carbides were to form ahead of the solidifying primary dendrite tips, they would sink and coalesce due to gravitational forces, which are antiparallel to the solidification direction. The interaction of the solid carbide particles and the advancing solid/liquid interface may potentially result in drag forces that inhibit the formation of convective channels. However, it is still unclear when precipitation of the blocky carbides occurs. While their composition and morphology suggest that precipitation occurs in the liquid, detecting their formation in the DTA and evaluating their role in affecting viscosity and local fluid-flow conditions is difficult due to their small volume fraction. The magnitude of the endothermic peak corresponding to the solvus temperature of these blocky carbides may be too small to detect and can be easily masked by other transformations, particularly the script and nodular carbides.

In previous studies of carbide morphologies in Ni-based alloys, blocky and script carbides were reported to exhibit similar growth characteristics regardless of composition.[23,39–41] The morphologies of script and blocky Ti or Nb-rich MC carbides were determined to be governed by the solidification parameters G and R.[40,41] However, the presence of three distinct Ta-rich MC carbide morphologies characterized in the alloys from the present study does not adhere to these conventional relationships. First, the nodular MC carbide morphology seems to be unique to Ni-based alloys containing Ta-rich MC carbides and has not been reported in alloys that contain Ti, Nb, or Hf-rich MC carbides. Under constant G and R values, carbide morphologies that are constrained by the surrounding dendritic structure can be affected by changes in composition, which drastically increase or decrease the solidus and liquidus temperatures of the alloy. As reported by Quested, it seems likely that carbide morphology is not simply a function of the solidification parameters, but is also influenced significantly by subtle chemical changes during solidification.[39]

Extensive investigations of freckling in transparent and binary alloy systems have shown that the onset of thermosolutal convection occurs in the upper portion of the mushy zone, where the fraction of solid is no greater than 0.5 to 0.6[1,6–8] At a higher fraction of solid, the permeability of the dendritic network is too low for solute-driven fluid flow to develop. According to Eq. [1], the permeability of the upper regions of the mushy zone is directly proportional to the solutal Rayleigh number for the onset of convective fluid flow. Changes in the upper regions of the mushy zone, such as the formation of dense carbide networks, should, in principle, lower the permeability and diminish the tendency for freckling. Accordingly, carbide precipitation closest to the liquidus would be expected to provide the most benefit in altering the permeability of the mushy zone, where convective cells are likely to develop. In this study, all of the alloys in which carbide dissolution was observed to occur close to the liquidus temperature ($\Delta T < 11$ °C) have essentially zero grain defects (Figure 11). For this set of alloys, the absence of freckle chains cannot be attributed entirely to the presence of carbide, because a number of these alloys also have elevated levels of tantalum (9.0 wt pct), which is also beneficial in reducing grain defects. However, comparison of the results from alloys containing 6.0 wt pct Ta does suggest a trend between freckling and the relative carbide precipitation temperature. This correlation is currently being investigated in greater detail through a separate study involving single-crystal alloys with nominally identical levels of tantalum and carbon.

To summarize, the results of this study clearly demonstrate that the presence of carbon lowers the tendency for grain-defect formation during solidification of high-refractory nickel-based single crystals. The carbon additions alter the segregation behavior of elements known to influence the onset of convective instabilities in carbon-free alloys, including Re, Ta, and W. Carbon additions also result in the precipitation of carbides near the liquidus temperature. Due to inadequate knowledge of the dependence of liquid density on composition and the degree to which the presence of carbides affects fluid flow and/or liquid properties, it is difficult to isolate the mechanism(s) by which carbon suppresses defect formation. Although it is likely that having the carbon in solution and precipitating carbides near the liquidus both contribute to preventing the breakdown of single-crystal solidification, it may be possible to assess these effects individually through further systematic changes in alloy chemistry; such experiments are in progress. Finally, it is worth noting that making relatively minor changes in alloy composition through carbon additions is a promising approach to developing new alloys that are amenable to low-gradient solidification.

V. CONCLUSIONS

1. Carbon additions to high-refractory, single-crystal Ni-based superalloys are beneficial in lowering the tendency for the development of freckle-type defects during unidirectional solidification under relatively low thermal-gradient conditions.
2. For the range of compositions investigated, intentional carbon additions resulted in the formation of three Ta-rich carbide morphologies: blocky, script, and nodular. Precipitation of script and nodular carbides occurred below the liquidus temperature in the mushy zone during solidification.
3. A slightly lower degree of tantalum, tungsten, and rhenium segregation was measured in as-cast alloys with

intentional carbon additions. Regardless of carbide morphology, the distribution coefficients of refractory elements (Ta, W, and Re) in alloys containing carbon were lower than comparable alloys containing no carbon additions.

4. Carbon, aluminum, and tantalum additions lower the liquidus temperature, while tungsten and rhenium additions modestly increase the liquidus temperatures for the range of compositions investigated.
5. Carbide precipitation temperatures are less sensitive to shifts in bulk composition than the solidus and liquidus temperatures.

ACKNOWLEDGMENTS

The authors acknowledge useful discussions with S.C. Huang, L. Rishel, M.F.X. Gigliotti, and W. King. The support provided by the General Electric Company along with NSF Grant No. DMR-9807648 is also gratefully acknowledged.

REFERENCES

1. S.M. Copley, A.F. Giamei, S.M. Johnson, and M.F. Hornbecker: *Metall. Trans.*, 1970, vol. 1, pp. 2193-2204.
2. T.M. Pollock, W.H. Murphy, E.H. Goldman, D.L. Uram, and J.S. Tu: in *Superalloys 1992*, S.D. Antolovich, R.W. Stusrud, R.A. MacKay, D.L. Anton, T. Khan, R.D. Kissinger, and D.L. Klarstrom, eds., TMS, Warrendale, PA, 1992, pp. 125-34.
3. T.M. Pollock and W.H. Murphy: *Metall. Mater. Trans.*, 1996, vol. 27A, pp. 1081-94.
4. A.F. Giamei and B.H. Kear: *Metall. Trans.*, 1970, vol. 1, pp. 2185-92.
5. R. Mehrabian, M.A. Keane, and M.C. Flemings: *Metall. Trans.*, 1970, vol. 1, pp. 3238-41.
6. A.K. Sample and A. Hellawell: *Metall. Trans. A*, 1984, vol. 15A, pp. 2163-73.
7. J.R. Sarazin and A. Hellawell: *Metall. Trans. A*, 1988, vol. 19A, pp. 1861-71.
8. M.C. Schneider, J.P. Gu, C. Beckermann, W.J. Boettinger, and U.R. Kattner: *Metall. Mater. Trans. A*, 1997, vol. 28A, pp. 1517-31.
9. F.L. VerSynder: U.S. Patent 3,260,505, 1966.
10. F.L. VerSnyder and M.E. Shank: *Mater. Sci. Eng.*, 1970, vol. 6, pp. 213-47.
11. K.O. Yu, J.J. Nichols, and M. Robinson: *JOM*, 1992, vol. 44, vol. 6, pp. 21-25.
12. K.O. Yu, J.A. Oti, M. Robinson, and R.G. Carlson: in *Superalloys 1992*, S.D. Antolovich, R.W. Stustrud, R.A. MacKay, D.L. Anton, T. Khan, R.D. Kissinger, and D.L. Klarstrom, eds., TMS, Warrendale, PA, 1992, pp. 134-44.
13. J.S. Tu and R.K. Foran: *JOM*, 1992, vol. 44, vol. 6, pp. 26-28.
14. A.L. Purvis, C.R. Hanslits, and R.S. Diehm: *JOM*, 1994, vol. 46, vol. 1, pp. 38-41.
15. P. Auburtin and A. Mitchell: in *Liquid Metals Processing*, AVS, Santa Fe, NM, 1996, pp. 18-34.
16. J.D. Hunt: *Mater. Sci. Eng.*, 1984, vol. 65, pp. 75-83.
17. T.M. Pollock: *Mater. Sci. Eng.*, 1995, vol. B32, pp. 255-66.
18. J.P. Gu, C. Beckermann, and A.F. Giamei: *Metall. Mater. Trans. A*, 1997, vol. 28A, pp. 1533-42.
19. M. Meyer ter Vehn, D. Dedecke, U. Paul, and P.R. Sahm: in *Superalloys 1996*, R.D. Kissinger, D.J. Deye, A.L. Anton, A.D. Cetel, M.V. Nathal, T.M. Pollock, and D.A. Woodford, eds., TMS, Seven Springs, PA, 1996, pp. 471-79.
20. S.D. Felicelli, D.R. Poirier, and J.C. Heinrich: *J. Cryst. Growth*, 1997, vol. 177, pp. 145-61.
21. S.R. Corriell, M.R. Cordes, W.J. Boettinger, and R.F. Sekerka: *J. Cryst. Growth*, 1980, vol. 49 (13).
22. C.T. Sims, N.S. Stoloff, and W.C. Hagel: *Superalloys II*, John Wiley & Sons, New York, NY, 1986.
23. J.K. Tien and T. Caulfield: *Superalloys, Supercomposites and Superceramics*, Academic Press, Inc., New York, NY, 1988.
24. M. Gell, D.N. Duhl, and A.F. Giamei: in *Superalloys*, J.K. Tien, S.T. Wlodek, H. Morrow, M. Gell, and G.E. Maurer, eds., ASM, Seven Springs, PA, 1980, pp. 205-14.
25. K. Harris and G.L. Erickson: U.S. Patent 4,582,548, 1986.
26. E.W. Ross, C.S. Wukusick, and W.T. King: U.S. Patent 5,399,313, 1995.
27. J.R. Mihalisin, J. Corrigan, R.J. Baker, E.L. Leonard, and J.L. Vandersluis: U.S. Patent 5,549,765, 1996.
28. M.J. Donachie: *J. Testing Eval.*, 1978, vol. 6 (3), pp. 189-915.
29. M.N. Gungor: *Metall. Trans.*, 1989, vol. 20A, pp. 2529-33.
30. S.C. Huang, L. Peluso, and D. Backman: in *Solidification 1999*, W.H.R. Hofmeister, J.R. Singh, N.B., Marsh, S.P., and Vorhees, P.W., eds., TMS, Warrendale, PA, 1999, pp. 163-72.
31. L. Nastac, L.S. Chou, and Y. Pang: in *Liquid Metals Processing*, AVS, Santa Fe, NM, 1999, pp. 207-23.
32. R. Sellamuthu and A.F. Giamei: *Metall. Trans. A*, 1986, vol. 17A, pp. 419-28.
33. W.A. Tiller: *The Science of Crystallization*, Cambridge University Press, Cambridge, United Kingdom, 1991.
34. P.K. Sung, D.R. Poirier, and E. McBride: *Mater. Sci. Eng.*, 1997, vol. A231, pp. 189-97.
35. T. Iida and R.I. Guthrie: *The Physical Properties of Liquid Metals*, Clarendon Press, Oxford, United Kingdom, 1988, pp. 70-73.
36. M.R. Jackson: *Metall. Trans. A*, 1977, vol. 8A, pp. 905-13.
37. V.A. Willis and D.G. McCartney: *Mater. Sci. Eng.*, 1991, vol. A145, pp. 223-32.
38. E. Fras, E. Guzik, W. Kapturckiewicz, and H.F. Lopez: *J. Mater. Eng. Performance*, 1996, vol. 5 (1), pp. 103-10.
39. P.N. Quested and M. McLean: *Mater. Sci. Eng.*, 1984, vol. 65, pp. 171-80.
40. A.K. Bhambri, T.Z. Kattamis, and J.E. Morral: *Metall. Trans. A*, 1975, vol. 6B, pp. 523-37.
41. R. Fernandez, J.C. Lecomte, and T.Z. Kattamis: *Metall. Trans. A*, 1978, vol. 9A, pp. 1381-86.
42. R. Elliot: *Eutectic Solidification Processing: Crystalline and Glassy Alloys*, Butterworth and Co., London, 1983, p. 370.